Ceramics International 46 (2020) 21560–21568

Contents lists available at ScienceDirect

Ceramics International

journal homepage: www.elsevier.com/locate/ceramint

F enhanced luminescence performance of $SrLu_2O_4:Ce^{3+}$ glass ceramic for superior high-power artificial horticultural LEDs

Mingcai Li[a], Xuejie Zhang[a,b], Yinjian Zheng[c], Yaliang Xu[c], Haoran Zhang[a,b], Yingliang Liu[a,b,**], Bingfu Lei[a,b,*]

[a] Key Laboratory for Biobased Materials and Energy of Ministry of Education, Guangdong Provincial Engineering Technology Research Center for Optical Agriculture, College of Materials and Energy, South China Agricultural University, Guangzhou, 510642, PR China
[b] Guangdong Laboratory of Lingnan Modern Agriculture, Guangzhou, 510642, PR China
[c] Institute of Urban Agriculture, Chinese Academy of Agricultural Sciences, Chengdu, 610213, PR China

ARTICLE INFO

Keywords:
Phosphor
Thermal stability
Glass ceramic
Plant growth LEDs

ABSTRACT

The discovery of light converter excited by near-ultraviolet (UV) superior broadband blue-emitting lighting source is a main challenge in plant growth LEDs. In this study, $SrLu_2O_4:Ce^{3+}$, Li^+, F^- blue phosphor has been synthesized via a solid-state reaction. Benefitting from doping of F^- ions, $SrLu_2O_4:Ce^{3+}$, Li^+, F^- phosphor (λ_{ex} = 405 nm, λ_{em} = 460 nm) shows a strong broadband (FWHM = 90 nm) blue-emitting with lower critical concentration of Ce^{3+} ions and an increasing 6.9% thermal quenching performance (92.1% @ 423 K of the peak intensity at room temperature). Moreover, a blue light converter composed of $SrLu_2O_4:Ce^{3+}$, Li^+, F^- phosphor and glass matrix is obtained based on phosphor-in-glass (PiG) technology, exhibiting excellent thermal stability and outstanding moisture resistance. A red light converter with commercial red phosphor is obtained by the same method. Furthermore, by combining of two light converters with near-UV chip, a proof-of-concept plant growth high power LED is achieved and applied in indoor Italian lettuce growing in comparison with commercial plant lamps.

1. Introduction

Crop failure due to unpredictable climate change and threat of pests and diseases is a worldwide challenge [1]. Traditional agriculture is mostly limited by climate, the large-scale use of inorganic fertilizers and pesticides, which result in a serious destruction of the environment and the decline of the yield of agricultural products. It also promotes the progress of indoor planting technology, making greenhouse planting and environmentally controllable indoor planting a reliable and sustainable way of crop production [2]. Light is one of the essential conditions for plant growth, which controls much plant metabolism and growth process [3]. For indoor planting technology, light source is a significant factor that restricts the development of indoor agriculture. Nowadays, artificial light sources (high-pressure sodium lamps, fluorescent lamps, metal halide lamps, and incandescent lamps) still have shortcomings such as low luminous efficiency, high energy consumption, and poor spectral matching [4]. The development of energy-saving and high-efficiency light sources is an important problem that needs to be solved in the development of plant factories [5]. Therefore, the development of high-efficiency energy-saving light source is an indispensable issue in the indoors agricultural field.

In recent years, with the advent of new semiconductor materials and optoelectronic technology, great improvement in the luminous efficiency of Light Emitting Diode (LED) has taken place [6]. LED applied in plant factories has been receiving widespread attention in countries around the world [7]. With the advantages of small size, long life, low heat generation, and wavelength adjustability, LED is an effective alternative light source for artificial light [8]. At present, the most popular mode of realizing LED illumination for plant illumination is that the blue LED chip or the near-ultraviolet LED chip excites the phosphor to generate blue and red light. In the next few decades, phosphor for plant lighting will also be one of the significant raw materials [9].

For plant growth, the blue light that the optimal wavelength range is 400–500 nm, has an important role in promoting leaf growth and

* Corresponding author. Key Laboratory for Biobased Materials and Energy of Ministry of Education, Guangdong Provincial Engineering Technology Research Center for Optical Agriculture, College of Materials and Energy, South China Agricultural University, Guangzho,u, 510642, PR China.
** Corresponding author. Key Laboratory for Biobased Materials and Energy of Ministry of Education, Guangdong Provincial Engineering Technology Research Center for Optical Agriculture, College of Materials and Energy, South China Agricultural University, Guangzho,u, 510642, PR China.
E-mail address: tleibf@scau.edu.cn (B. Lei).

https://doi.org/10.1016/j.ceramint.2020.05.259
Received 14 April 2020; Received in revised form 15 May 2020; Accepted 25 May 2020
Available online 31 May 2020

accumulating protein and non-carbohydrate [10]. At present, the research on phosphor for plant lighting pays attention to red light, and has also made prominent progress, such as $3.5MgO•0.5MgF_2•GeO_2:Mn^{4+}$, $CaAlSiN_3:Eu^{2+}$ and $Sr_2Si_5N_8:Eu^{2+}$ phosphors [11]. However, there are fewer studies on blue light-emitting phosphor. The blue light currently reported for applying in plant illumination is mainly provided by LED chips of 420 nm or 460 nm, but it does not well meet the demand for blue light by photosynthetic pigments due to the disadvantage of a narrow full-width at half-maximum (FWHM) [12]. For phosphors applied in blue light plant lighting, the most suitable candidate is $BaMgAl_{10}O_{17}:Eu^{2+}$ blue phosphor, but there is still the disadvantage that ultraviolet light excitation inhibits plant growth [13]. In order to solve this problem, it is urgent to develop blue phosphors excited by near-ultraviolet light.

Zheng et al. reported in 2016 the $Ca_2LuZrScAl_2GeO_{12}$: Ce^{3+} phosphor [14]. Although it's capable of matching near-ultraviolet excitation and emitting blue light, it has poor thermal stability that the fluorescence intensity drops to 50% of room temperature at 90 °C, which is inconsistent with the requirements of plant lighting. Zhong et al. reported in 2016 that $Ca_3Zr_2SiGa_2O_{12}$: Ce^{3+} blue phosphor have better thermal stability than the former, but the fluorescence intensity has dropped to 50% of room temperature at 150 °C, which is also inconsistent with the demand for high-power plant lighting [15]. Hao et al. reported in 2017 that $CaO:Eu^{2+}$ blue phosphor can still maintain room temperature fluorescence intensity of 91% of room temperature at 150 °C, but CaO with prone to moisture absorption have poor chemical stability, which still does not meet the requirements of plant lighting [16]. Until 2018, Hao et al. reported that $SrLu_2O_4:Ce^{3+}$ blue phosphor, whether excited or emitted, can match the requirements of plant lighting, and fluorescence intensity maintains 86% of the room temperature at 150 °C, which is basically accords with the requirement of phosphor applied in plant lighting, but the disadvantage is that the fluorescence intensity is relatively low, and thermal stability needs to be improved [17].

In this work, by regulating the structure of $SrLu_2O_4:Ce^{3+}$, with a certain concentration of F^- ions doped, the fluorescence intensity and thermal stability are significantly improved. In addition, it is fabricated into high-power plant lighting device by phosphor-in-glass (PiG) technology. Plant cultivation experiment showed that the $SrLu_2O_4$: Ce^{3+}, Li^+, F^- phosphor was used to provide blue light and the biomass of plants was significantly improved.

2. Experimental

2.1. Sample preparation

The powder samples of $SrLu_2O_4$: xCe^{3+}, xLi^+, $4xF^-$ (x = 0.0001, 0.0002, 0.0003, 0.0004, 0.0005, 0.0006, 0.0007, 0.0008) were prepared by a solid-state reaction. The stoichiometric amounts of Lu_2O_3 (99.99%, Aladdin), $SrCO_3$ (99.99%, Aladdin), CeO_2 (99.99%, Aladdin), Li_2CO_3 (99.99%, Aladdin) and NH_4F (99.99%, Aladdin) as raw materials, were homogeneously ground for 1/2 h, respectively, and then mixtures sintered in a tube furnace at 4 °C min^{-1} to 1500 °C for 6 h under a reducing atmosphere H_2–N_2 (5%). The as-obtained samples were cooled naturally to room temperature and were reground into powder for subsequent tests. The samples without F^- ions doped of $SrLu_2O_4:yCe^{3+}$, yLi^+, (y = 0.0005, 0.001, 0.002, 0.003, 0.004, 0.005, 0.006, 0.007, 0.008) were synthesized via the same methods as the references. Phosphor-in-glass (PiG) samples were synthesized with glass matrix composition of $30SiO_2$–$30ZnO$–$22B_2O_3$–$12NaO$–$6Al_2O_3$, which phosphor and glass matrix were pressed into cylinder and sintered for 1/2 h at 580 °C in air atmosphere. PiG-plant lamp was fabricated using the blue $SrLu_2O_4$: Ce^{3+}, Li^+, F^--PiG, commercial $3.5MgO•0.5MgF_2•GeO_2:Mn^{4+}$ (purchased from Jiangmen Kanhoo Industry Co., Ltd) -PiG and near-UV LED chip (Model JL-2835-60 W, purchased from JinLei Agricultural Tech. Co., LTD).

2.2. Plant cultivation

Hydroponics cultivation experiments of Italian lettuce were carried out under PiG-plant lamps and the commercial plant lamps using Hoagland solution. The Italian lettuces were grown under two different light sources for 24 days with light intensity is 130 μmol m^{-2}·s^{-1} PPFD. The planting conditions were 25 °C, 400 ppm CO_2 and 58% humidity.

2.3. Characterizations

The XRD patterns date were performed (Bruker Corporation, Germany) operating at 40 kV and 40 mA with monochromatized Cu Kα radiation (λ = 1.5405 Å). The morphology and elemental composition were measured by scanning electron microscope (SEM), equipped with energy dispersive X-ray spectroscopy (EDS) system (Hitachi SU8220, Japan). The confocal laser scanning microscope (CLSM) images were collected with a confocal laser scanning microscope (CLSM 710, Zeiss), equipped with a 405 nm laser as an excitation source. The photoluminescence excitation (PLE) and photoluminescence (PL) spectra and the temperature range of RT-200 °C were measured using a Hitachi F-7000 Fluorescence Spectrometers equipped with a 150 W xenon lamp as an excitation source.

3. Results and discussion

Based upon the appropriate photoluminescence properties, the photoluminescence excitation (PLE) and photoluminescence (PL) spectra of $SrLu_2O_4$: Ce^{3+}, Li^+, F^- phosphor are a proper alternative for application in 405 nm near-ultraviolet (UV) light excited plant growth LEDs. The emission of broad-band is matched well with the absorption band of photosynthetic pigments under the excitation of near-UV. As shown in Fig. 1a, since Ce^{3+} ion valence state and ion radius are similar to Lu^{3+} ion, Ce^{3+} ion will enter the main lattice of $SrLu_2O_4$ replaced the Lu^{3+} ion position in the host matrix. The emission spectra of $SrLu_2O_4$: Ce^{3+}, Li^+, F^- reveal an asymmetric broadband at 460 nm arising from the 4f [1]→5 d^1 transition of Ce^{3+}, with a FWHM of ~90 nm under 405 nm excitation, which can be well fitted into two Gaussian bands peaking at 20256 cm^{-1} (T_{2g}→$^2F_{7/2}$) and 22168 cm^{-1} (T_{2g}→$^2F_{5/2}$) [18]. The different energy between the two sublevels separated by 1912 cm^{-1} are ascribed to spin-orbit coupling. Fig. 1b shows the PL intensity attaining a peak in $SrLu_2O_4$: xCe^{3+}, xLi^+, $4xF^-$ phosphor with the doping concentration of x = 0.0005, while the critical concentration of $SrLu_2O_4$: xCe^{3+}, xLi^+ phosphor is 0.002. It is noteworthy that the difference between the critical concentrations in both is approximately 4 times, and $SrLu_2O_4$: Ce^{3+}, Li^+, F^- phosphor reveals higher intensity, indicating that F^- ions play a crucial role in activating Ce^{3+} ions in $SrLu_2O_4$ host. The energy transfers mechanism accounting for concentration quenching with the help of the critical distance (R_c) can be figured out, which R_c calculated by the following formula [19,20]:

$$R_c = 2\left(\frac{3V}{4\pi x_c N}\right)^{1/3} \quad (1)$$

x_c on behalf of critical doping concentration of Ce^{3+} ion, V on behalf of the unit cell volume, and N on behalf of the number of unit cell sites occupied by Ce^{3+}. The both lattice parameters can be detailed in Table 1, which are derived from Rietveld structure refinements. The values of R_c for $SrLu_2O_4$: xCe^{3+}, xLi^+, $4xF^-$ (x = 0.0005) and $SrLu_2O_4$: xCe^{3+}, xLi^+ (y = 0.002) are 49.978 Å and 31.465 Å, respectively, indicating the types of concentration quenching mechanism of both pertain to multipole–multipole interaction [21]. Furthermore, energy transfer mechanism can be divided into diverse types based on the Dexter theory, and identified via the following formula [22].

$$I/x = kx)(x)(x)^{\theta/3}]^{-1} \quad (2)$$

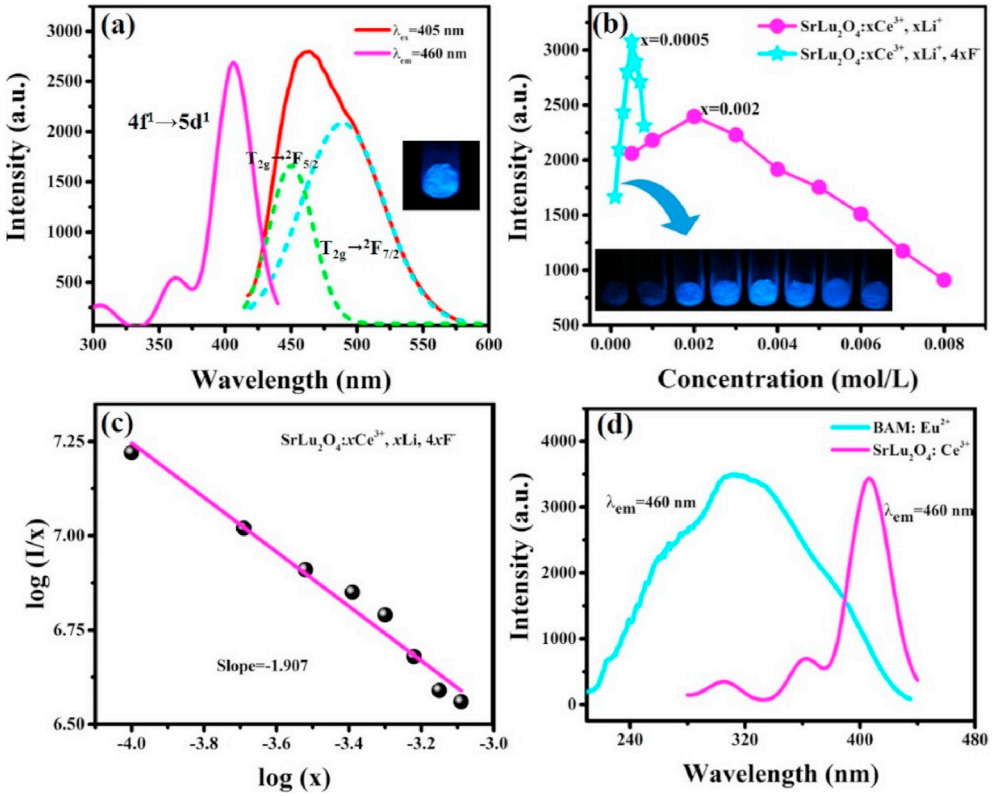

Fig. 1. (a) PLE and PL spectra of $SrLu_2O_4$: $0.0005Ce^{3+}$, $0.0005Li^+$, $0.002F^-$ phosphor. Inset shows photograph of $SrLu_2O_4$: Ce^{3+}, Li^+, F^- under 365 nm UV light. (b) PL emission intensity with different x in $SrLu_2O_4$: xCe^{3+}, xLi^+, $4xF^-$. Insets show photographs of $SrLu_2O_4$: Ce^{3+}, Li^+, F^- with various doping concentration x under 365 nm UV light. (c) log(I/x) as a function of doping concentration x in $SrLu_2O_4$: xCe^{3+}, xLi^+, xF^-. (d) Comparation of PLE and PL spectra of $SrLu_2O_4$: Ce^{3+}, Li^+, F^- and BAM: Eu^{2+} phosphors.

Table 1
Rietveld structure refinement data for $SrLu_2O_4$: xCe^{3+}, xLi^+, $4xF^-$ (x = 0.0005) and $SrLu_2O_4$: yCe^{3+}, yLi^+ (y = 0.002).

Sample	Phase	Space group	Cell parameters (Å)	Cell volume (Å^3)	Z	R_B (%)	R_{wp} (%)	R_p (%)	χ [2]
1	$SrLu_2O_4$: Ce^{3+}, Li^+, F^-	Pnam	a = 9.9796 (1) b = 11.7550 (2) c = 3.34145 (4)	V = 391.985 (9)	12	1.80	6.96	5.07	1.92
2	$SrLu_2O_4$: Ce^{3+}, Li^+	Pnam	a = 9.9716 (1) b = 11.7488 (1) c = 3.33965 (4)	V = 391.256 (8)	12	3.95	9.26	6.58	2.30

I represents the PL intensity, x represents activator Ce^{3+} ion concentration, k and β are constants, and θ are several values such as 3, 6, 8 or 10, which represent the energy migration among nearest neighbor or next nearest neighbor activators, dipole-dipole, dipole-quadrupole, or quadrupole-quadrupole interaction [23]. Fig. 1c shows that the relationship between log [x] and log [I/x], fitting the slope ($\theta/3$) is −1.907. Thus, the value of θ calculated to 5.721 (proximity to 6) demonstrate that concentration quenching of Ce^{3+} doping $SrLu_2O_4$ majorly derive from interactions between of dipole-dipole. The results are consistent with other reports with no-doping F^- [24]. In other words, the doping of F^- ions unaltered the phosphor's concentration quenching, but obtain more low critical concentration. Besides, compared with BAM: Eu^{2+} commercial phosphor, PLE spectra of $SrLu_2O_4$: Ce^{3+}, Li^+, F^- is more suitable for the demand of near-UV excitation, and PL intensity is 78.2% stronger than the former, as shown in Fig. 1d [25].

Fig. 2a shows the scanning electron microscope (SEM) images of $SrLu_2O_4$: Ce^{3+}, Li^+, F^- phosphor, in which the particle size is about 3–5 μm with irregular shapes. Furthermore, the energy dispersive X-ray spectroscopy (EDS) elemental mapping technique was adopted to confirm the composition uniformity of $SrLu_2O_4$: Ce^{3+}, Li^+, F^- as shown in Fig. 2b–d. EDS mapping images show that Sr, Lu elemental are homogeneously around the particles, which further confirms that the prepared samples are $SrLu_2O_4$ crystals.

To explain the role of F^- ion in phosphor structurally, $SrLu_2O_4$: Ce^{3+}, Li^+ and $SrLu_2O_4$: Ce^{3+}, Li^+, F^- phosphors were measured by X-raw diffraction (XRD) for structural analysis. As can be seen from Fig. 3a, introduction of a small couple of Ce^{3+}, Li^+, F^- ions did not alter the rhombic crystal structure of $SrLu_2O_4$ sample. The sample was homogeneous with the same diffraction peak and good crystallinity, matching with $SrLu_2O_4$ phase standard card (JCPDS#32–1242). But for details of the amplified diffraction peak, the small angle shift is observed in the diffraction peak of the doped F^- ion sample (Fig. 3b). According to Bragg equation $2d\sin\theta = n\lambda$, the crystal plane spacing of $SrLu_2O_4$ increases with the shift of diffraction peak to the direction of small angle [26]. To further explore the causes, rietveld structure refinement was adopted. The results show that the cell parameters of $SrLu_2O_4$: Ce^{3+}, Li^+, F^- are larger than those of $SrLu_2O_4$: Ce^{3+}, Li^+. The specific details can be obtained from Table 1, which is corresponding to the small angle shift of diffraction peak in Fig. 3 b. Inside the $SrLu_2O_4$: Ce^{3+}, Li^+, F^- phosphor, Ce^{3+} ion occupies a position of Lu^{3+} ion, while Li^+ ion is a charge donor to charge balance, thus improving the fluorescence efficiency of $SrLu_2O_4$: Ce^{3+}, Li^+ [27]. In addition, the unit cell volume of $SrLu_2O_4$: Ce^{3+}, Li^+, F^- is slightly larger

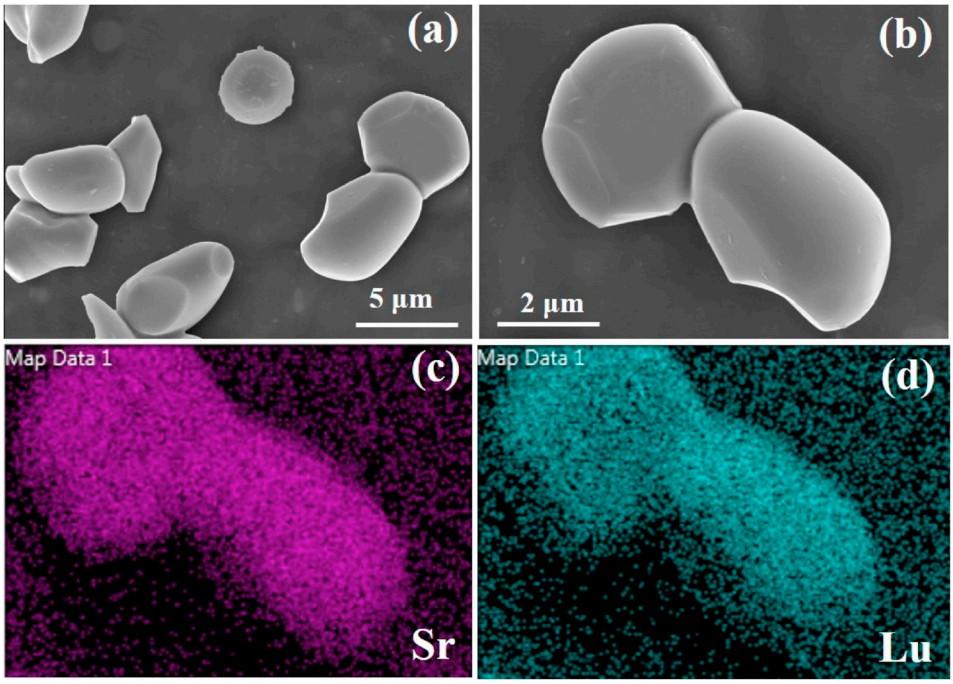

Fig. 2. (a) SEM image of $SrLu_2O_4$: 0.0005Ce^{3+}, 0.0005Li^+, 0.002F^- phosphor microcrystal particles and b) an enlarged particle. (c–d) Element mapping images of Sr and Lu.

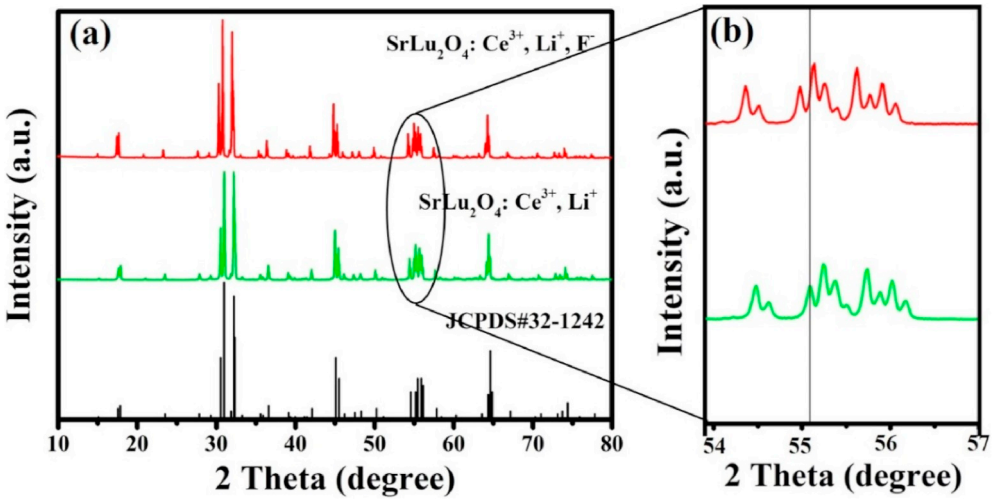

Fig. 3. (a) XRD pattern of $SrLu_2O_4$: Ce^{3+}, Li^+ and $SrLu_2O_4$: Ce^{3+}, Li^+, F^- phosphors. (b) Details of both XDR diffraction peaks.

than that of $SrLu_2O_4$: Ce^{3+}, Li^+, which is caused by the O^{2-} ion position being simultaneously occupied by two F^- ions [28]. The doping of the two F^- ions leads to a larger critical distance between the activated ions, triggering lower the critical concentration of Ce^{3+} ion. At the same time, due to the relatively large electronegativity of F^- ion, the doping of the two F^- ions are beneficial to enhance the local crystalline field, thereby enhancing the fluorescence intensity [29]. In summary, the enhancement of the luminescent property of $SrLu_2O_4$: Ce^{3+}, Li^+, F^- is caused by the doping of F^- ion, which leads to structural changes in the matrix and local crystalline field change.

The luminescence property can be improved by introducing F^- ion from the perspective of thermal stability. The temperature dependent spectra of $SrLu_2O_4$: Ce^{3+}, Li^+ and $SrLu_2O_4$: Ce^{3+}, Li^+, F^- phosphors can be obtained by variable temperature fluorescence characterization. As the ambient temperature increases, the fluorescence intensity of $SrLu_2O_4$: Ce^{3+}, Li^+ and $SrLu_2O_4$: Ce^{3+}, Li^+, F^- decreases due to the intensification of non-radiative transitions [30]. The details of the changes are available in Fig. 4a–b. As the temperature reach to 150 °C, the fluorescence intensities of $SrLu_2O_4$: Ce^{3+}, Li^+, F^- and $SrLu_2O_4$: Ce^{3+}, Li^+ maintain 92.1% and 85.2% compared with room temperature, respectively. The activation energy (*Ea*) of $SrLu_2O_4$: Ce^{3+}, Li^+, F^- is higher than that of $SrLu_2O_4$: Ce^{3+}, Li^+, indicating that the electrons of Ce^{3+} in $SrLu_2O_4$: Ce^{3+}, Li^+, F^- exist more effective excitation process and have lower thermal radiation energy as shown in Fig. 4c [31]. The activation energy (*Ea*) can be calculated according to the following formula [32]:

$$I(T) = \frac{I_0}{1 + Aexp\left(-\frac{E_a}{kT}\right)} \tag{3}$$

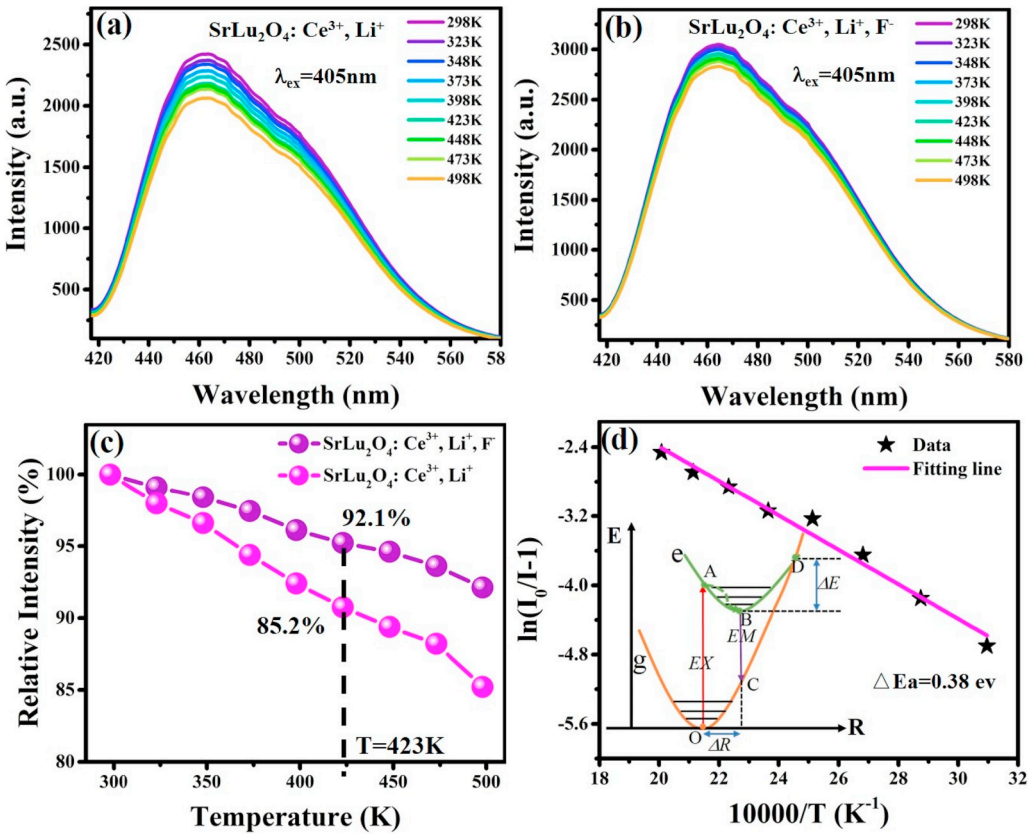

Fig. 4. Temperature dependent fluorescence intensity of (a) $SrLu_2O_4$: Ce^{3+}, Li^+ phosphor and (b) $SrLu_2O_4$: Ce^{3+}, Li^+, F^- phosphor. (c) Trend of fluorescence intensity from 298 to 423 K. (d) Activation energy of temperature dependent in $SrLu_2O_4$: Ce^{3+}, Li^+, F^- phosphor. The inset shows the schematic configuration coordinate diagram of the Ce^{3+} ion.

I_0 and $I(T)$ are the fluorescence intensities of the phosphors at room temperature and other temperatures, respectively, and both A and k are constant, where k is the Boltzmann constant. According to the results of calculation, the activation energy of $SrLu_2O_4$: Ce^{3+}, Li^+, F^- is 0.38 eV, outweighing the activation energy of $SrLu_2O_4$: Ce^{3+}, Li^+ (0.22 eV). To specifically describe thermal quenching process, a displacement coordinate model is created, as shown in the inset of Fig. 4d. The thermal quenching phenomenon of the sample is caused by non-radiative relaxation [33]. The ground state and the excited state can be expressed by two parabolas. The electrons in the ground state of O are excited to the excited state A, and the excited electrons are not radiated to B level. Finally, the radiation transition returns to the ground state and emits blue light peak at 460 nm. As the temperature increases, some electrons in the excited state absorb the additional activation energy and reach the intersection of the ground state and the excited state [34]. Then the electrons return to the ground state through the non-radiative transition, converting radiant energy into thermal energy, which leads to decrease in luminous intensity [35]. The material has a higher activation energy, indicating that the probability of non-radiative transition caused by its high temperature is small [36]. The above results reveal that $SrLu_2O_4$: Ce^{3+}, Li^+, F^- phosphor have better thermal stability, which is more suitable in high power plant lighting LED devices.

Luminescent materials applied in high power plant lighting LED must have excellent thermal stability to withstand high junction

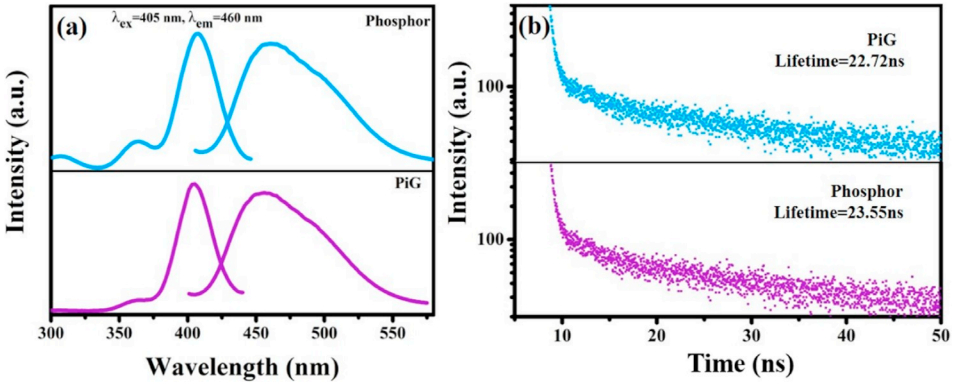

Fig. 5. (a) PLE and PL spectra of $SrLu_2O_4$: Ce^{3+}, Li^+, F^- phosphor and PiG. (b) Decay curves of $SrLu_2O_4$: Ce^{3+}, Li^+, F^- phosphor and PiG.

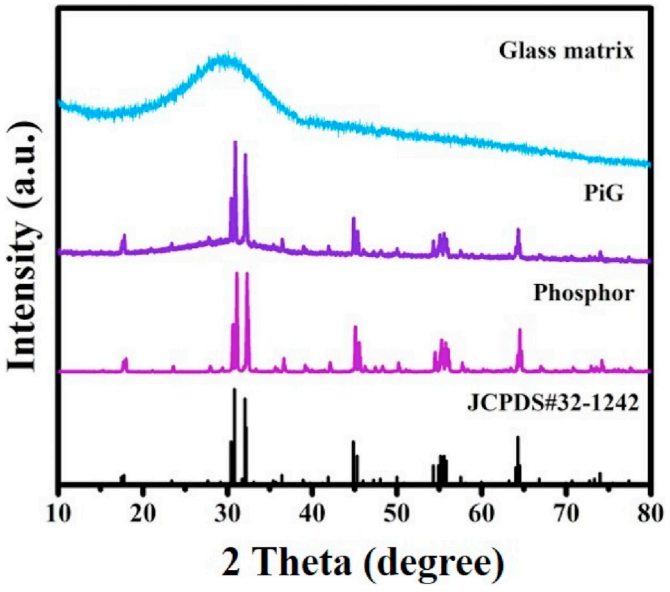

Fig. 6. XRD patterns of $SrLu_2O_4$: $0.0005Ce^{3+}$, $0.0005Li^{+}$, $0.002F^{-}$ phosphor, glass matrix, and PiG.

temperatures from the chip. Prepared by the phosphor-in-glass (PiG) technology can better solve the problems. Transparent SiO_2–ZnO–B_2O_3–Na_2O–Al_2O_3 glass matrix and $SrLu_2O_4$: Ce^{3+}, Li^{+}, F^{-} phosphor were used to co-sinter into a PiG material. The luminescence properties are compared between PiG and phosphor, which is an important mean to test the feasibility of PiG technology.

Fig. 5a shows the excitation and emission spectra of PiG and phosphor. The excitation spectra from 200 to 245 nm, 245–380 nm and 380–450 nm are attributed to the 4f [1]→5 d^1 transition of Ce^{3+} ion. The emission spectra of PiG include a 460 nm emission peak from Ce^{3+} ion T_2→^{2}F transition under excitation by 405 nm. By comparison, the shape and intensity of the excitation peak of PiG are smaller than that of the corresponding embedded phosphor, which is mainly caused by the certain absorption of the glass matrix [37]. The fluorescence lifetime curve of PiG and phosphor are shown in Fig. 5b. After fitting the curve, the fluorescence lifetime of the phosphor is 23.55 ns, while the fluorescence lifetime of PiG is 22.72 ns? Both are not obviously changed. The above results indicate that the luminescent properties of $SrLu_2O_4$: Ce^{3+}, Li^{+}, F^{-} phosphor are almost unchanged during the preparation of PiG.

Fig. 6 shows these XRD patterns of glass matrix, $SrLu_2O_4$: Ce^{3+}, Li^{+}, F^{-} phosphor and PiG. It can be found that the XRD pattern of PiG contains sharp diffraction peaks from $SrLu_2O_4$: Ce^{3+}, Li^{+}, F^{-} phosphor and broad peaks of the glass matrix. The distribution of $SrLu_2O_4$: Ce^{3+}, Li^{+}, F^{-} phosphor in PiG is presented in Fig. 7a. It can be seen from the SEM image that the irregular phosphor particles are distributed in the glass matrix. Fig. 7b–d show the mapping of the phosphor particles and the glass matrix elements. It further confirms that the phosphor and the glass matrix have good compatibility in the PiG. Fig. 7e shows the image of PiG token in daylight, in which the two-dimensional and three-dimensional distribution of fluorescence emission in the glass matrix was observed by a CLSM with a 405 nm excitation source. The results reveal that the $SrLu_2O_4$: Ce^{3+}, Li^{+}, F^{-} phosphor is evenly dispersed in the glass (Fig. 7f–g).

In order to further confirm the application possibility of PiG, the accelerated aging test was adopted to characterize its thermal stability and water resistance. The comparison of the luminescence intensity of PiG in 200 °C drying oven for 15 days before and after (Fig. 8a). The results show that there is almost unchanged in the luminescence intensity of PiG after 15 days in high temperature treatment. The luminescence contrast after placing the PiG in 85 °C water for 0, 10, 20, 30, 40, and 50 h (Fig. 8b). The results show that the luminescence intensity is also almost undiminished. These results all indicate that PiG is feasible in harsh practical application. To demonstrate the potential application in plant lighting, PiG-plant lamp was fabricated using the blue $SrLu_2O_4$:

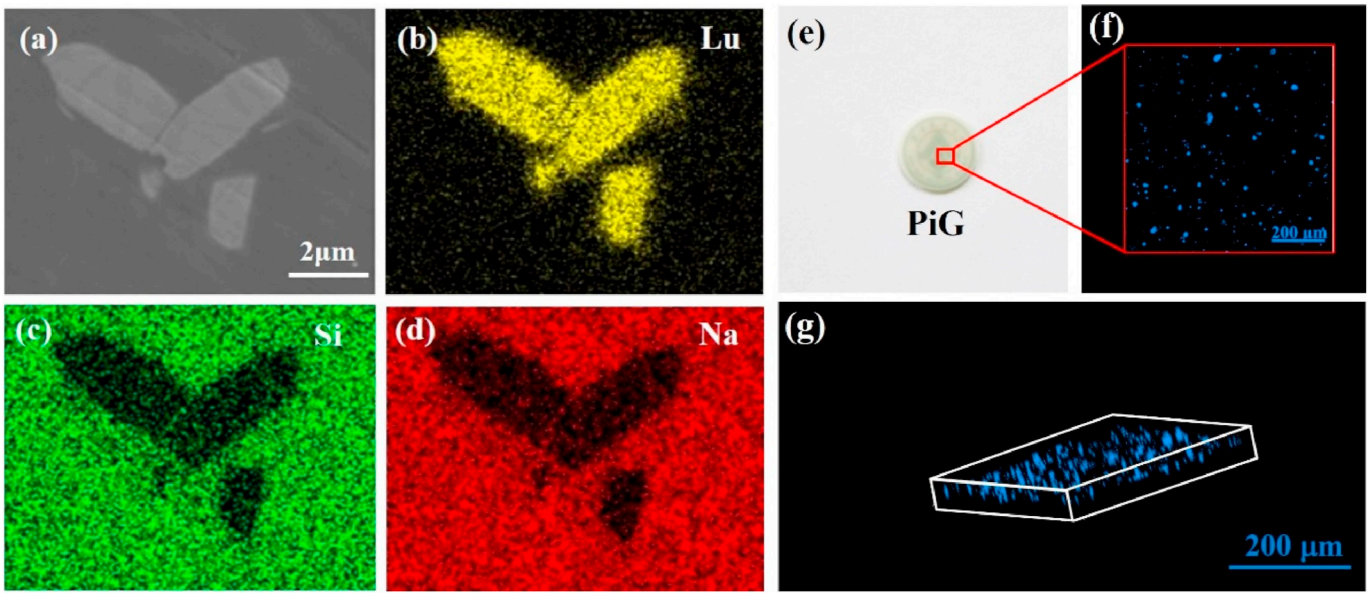

Fig. 7. (a–d) EDS mapping images of PiG. (e) Digital picture of PiG. (f–g) CLSM images of PiG.

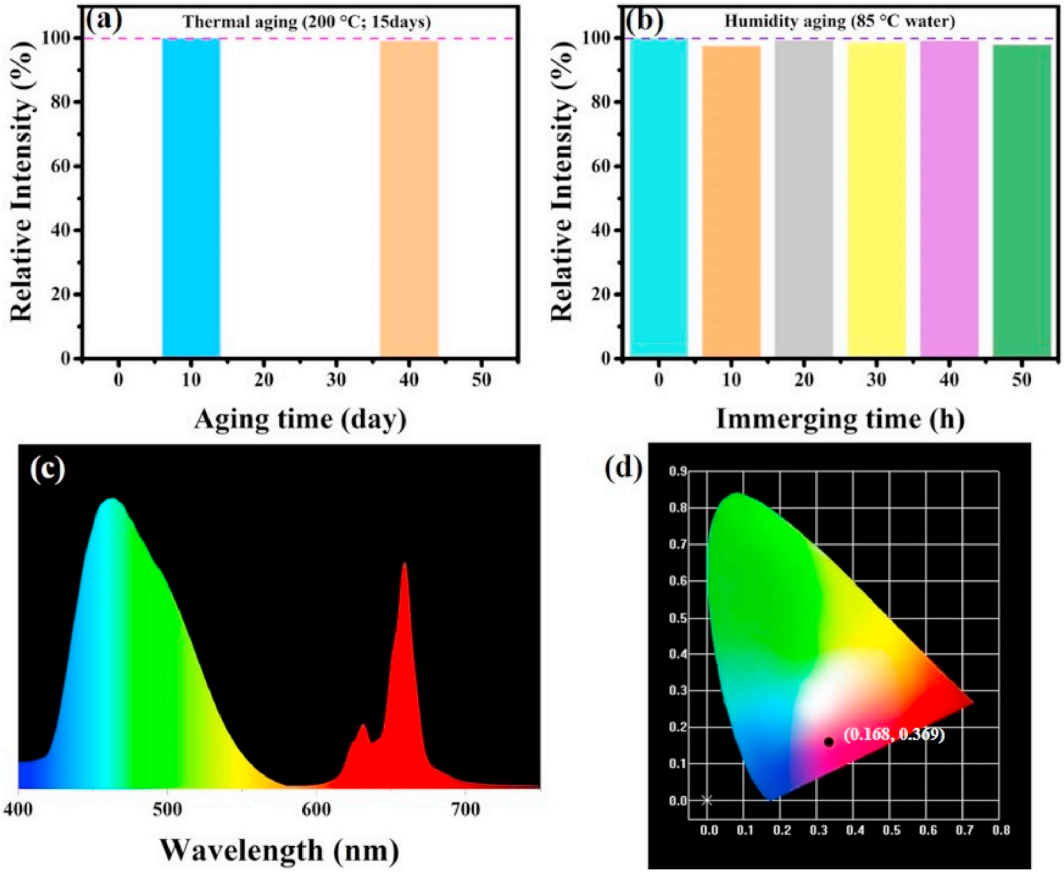

Fig. 8. (a) Integrated PL intensity change PiG before and after heat resistance test. (b) Alterations of relative PL intensities of PiG in humidity resistance test. (c) PL of PiG-plant lamp. (e) the color coordinates position of the PiG-plant lamp spectrum. (For interpretation of the references to colour in this figure legend, the reader is referred to the Web version of this article.)

Ce^{3+}, Li^{+}, F^{-}-PiG, commercial $3.5MgO{\bullet}0.5MgF_2{\bullet}GeO_2{:}Mn^{4+}$-PiG and near-UV LED chip (λ = 405 nm). Fig. 8c presents dual emission EL spectrum of PiG-plant lamp, and Fig. 8d shows the colour coordinates position of the dual emission spectrum.

To explore the application of PiG-Plant lamp in plant lighting, the Italian lettuce were cultured in plant factory with commercial plant lamps as reference, simulation diagram as shown in Fig. 9a. The spectra of PiG-Plant lamps and commercial plant lamps are spectra nearly overlap in the red region, while the spectrum of PiG-Plant lamps in the blue region are obviously wider than that of commercial plant lamp, achieving the desired effect that broadband blue light promotes plant growth (Fig. 9b). Observed after 24 days of cultivation, Samples-b (under PiG-Plant lamps) show more exuberant and verdant than Samples-a (under commercial plant lamps), as shown in Fig. 9c–d. Detailed photograph of represented samples with different treatments are obtained from Fig. 9e. In addition, the fresh weight, dry weight, plant height, and total chlorophyll content of Samples-a and Samples-b were measured respectively. The results show that Samples-an increase 13.5% more fresh weight, 24.4% more dry weight, 16.7% more plant height, and 5.8% more total chlorophyll content than Samples-b, more details can be seen in Table 2, Each Italian lettuce sample is planted with 24 pieces (4 * 6 arrangement). In order to prevent the edge effects, the outermost 16 pieces are removed, and the remaining 8 pieces are selected for the average growth of 5 pieces. It is testified that the PiG-Plant lamps is an excellent light source for improving plant growth [38–40].

4. Conclusion

In conclusion, a lutecium-based broadband blue-emitting $SrLu_2O_4{:}Ce^{3+}$, Li^{+}, F^{-} phosphor have been synthesized with λ_{em} = 460 nm, λ_{ex} = 405 nm and FWHM = 90 nm. After adding F^{-} ions, the critical concentration of doping of Ce^{3+} ions decreased 4 times, and the thermal stability is increased by 6.9%. Furthermore, a near-UV excited light converter haves been prepared by PiG technology with excellent thermal stability and outstanding moisture resistance, which optical properties are almost identical with that of phosphor. Finally, the growing experiments results show that plant height increased by 16.7%, fresh weight increased by 13.5%, dry weight increased by 24.4% and chlorophyll content increased by 5.8%. The above results suggest that the robust light converter is expected to be a potential candidate for 405 nm excited based plant growth LEDs.

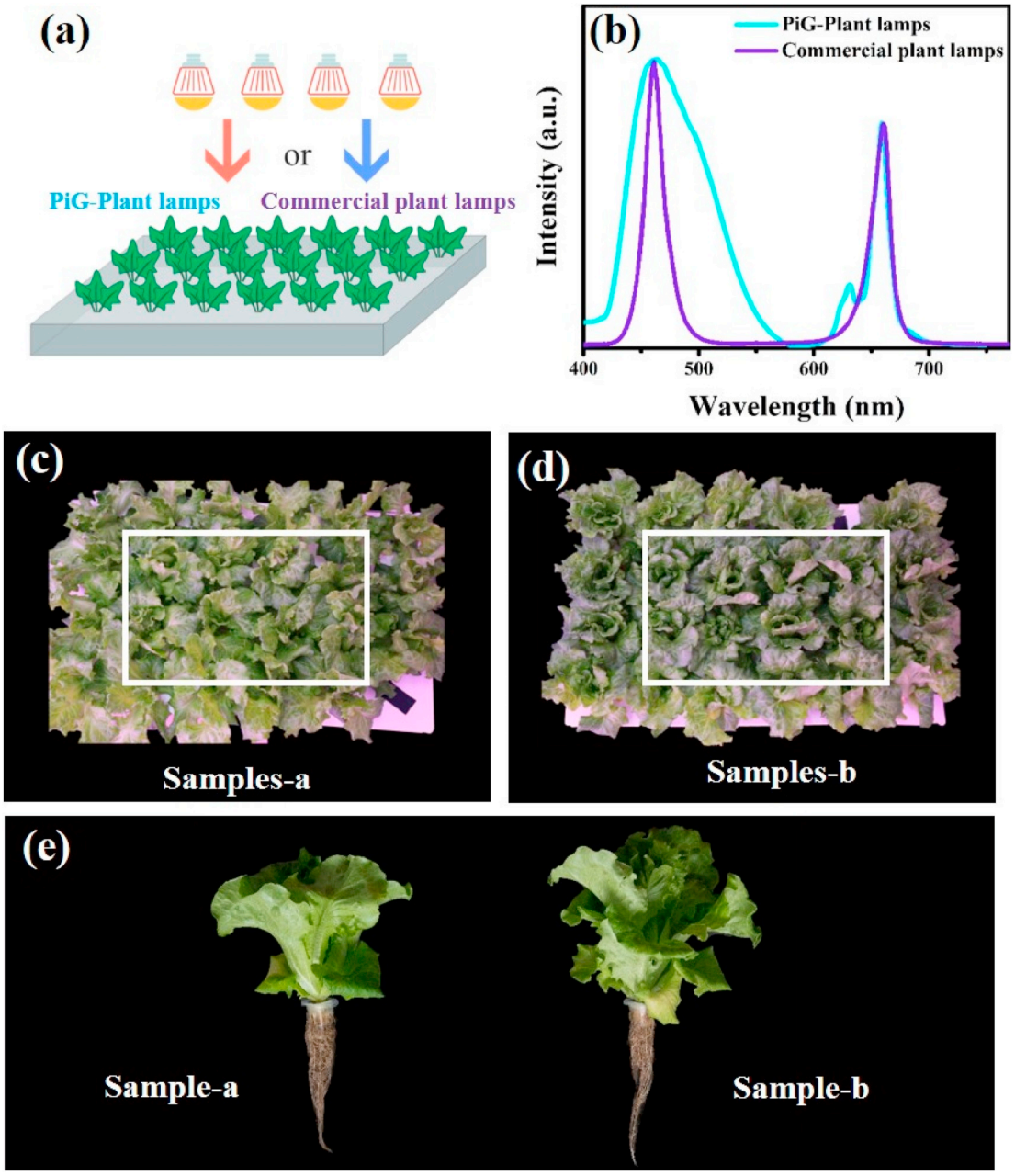

Fig. 9. (a) Schematic illustration of Plant cultivation. (b) EL spectra of PiG-plant lamps and commercial plant lamps. (c–d) The samples irradiated by different light sources after 24 days of cultivation. (e) The samples detail.

Table 2
Results of different light sources on various indexes of Italian lettuce.

Samples	Fresh weight (g·plant^{-1})	Dry weight (g·plant^{-1})	Plant height (cm)	Total chlorophyll content (mg·g^{-1})
A	55.74	1.97	17.32	0.6821
B	63.29	2.45	20.21	0.7221

Declaration of competing interest

There are no conflicts to declare.

Acknowledgements

The present work was supported by the National Natural Science Foundation of China (Grant No. 21671070); the Project of GDUPS (2018) for Prof. Bingfu LEI; the Guangzhou Science & Technology Project (No. 202007020005).

References

[1] A. Agarwal, S.D. Gupta, Impact of light-emitting diodes (LEDs) and its potential on plant growth and development in controlled-environment plant production system, Curr. Biotechnol. 5 (2016) 28–43.
[2] J. He, L. Qin, E.L.C. Chong, T.W. Chong, S.K. Lee, Plant growth and photosynthetic characteristics of mesembryanthemum crystallinum grown aeroponically under different blue and red-LEDs, Front. Plant Sci. 8 (2017) 1–13.
[3] S.D. Gupta, B. Jatothu, Fundamentals and applications of light-emitting diodes (LEDs) in in vitro plant growth and morphogenesis, Plant Biotechnology Reports 7 (2013) 211–220.
[4] M.R. Sabzalian, P. Heydarizadeh, M. Zahedi, High performance of vegetables, flowers and medicinal plants in a red-blue LED incubator for indoor plant production, Agron. Sustain. Dev. 34 (2014) 879–886.
[5] O. Długosz-Grochowska, A. Kołton, R. Wojciechowska, Modifying folate and polyphenol concentrations in Lamb's lettuce by the use of LED supplemental lighting during cultivation in greenhouses, J. Funct. Food 26 (2016) 228–237.
[6] S. Nadalini, P. Zucchi, C. Andreotti, Effects of blue and red LED lights on soilless cultivated strawberry growth performances and fruit quality, Eur. J. Hortic. Sci. 82 (2017) 12–20.
[7] Z. Zhou, M. Xia, Y. Zhong, S. Gai, S. Huang, Y. Tian, X. Lu, N. Zhou, Dy^{3+}@Mn^{4+} co-doped $Ca_{14}Ga_{10-m}Al_mZn_6O_{35}$ far-red emitting phosphors with high brightness and improved luminescence and energy transfer properties for plant growth LED lights, J. Mater. Chem. C 5 (2017) 8201–8210.
[8] M. Ashraf, P.J.C. Harris, Photosynthesis under stressful environments: an overview, Photosynthetica 51 (2013) 163–190.
[9] Y. Zheng, H. Zhang, H. Zhang, Z. Xia, Y. Liu, M.S. Molokeev, B. Lei, Co-substitution of Y^{3+}/Mg^{2+} for Ca^{2+}/Al^{3+} in $CaAl_{12}O_{19}$:Mn^{4+} phosphors: local structure evolution, photoluminescence tuning and application for plant growth LEDs, J. Mater. Chem. C 6 (2018) 4217–4224.
[10] T. Nakajima, T. Tsuchiya, Plant habitat-conscious white light emission of Dy^{3+} in whitlockitelike phosphates: reduced photosynthesis and inhibition of bloom impediment, ACS Appl. Mater. Interfaces 7 (2015) 21398–21407.
[11] M. Li, X. Zhang, H. Zhang, W. Chen, L. Ma, X. Wang, Y. Liu, B. Lei, Highly efficient and dual broad emitting light convertor: an option for next-generation plant growth LEDs, J. Mater. Chem. C 7 (2019) 3617–3622.
[12] J. Deng, H. Zhang, X. Zhang, Y. Zheng, J. Yuan, H. Liu, B. Lei, J. Qiu, Ultrastable red-emitting phosphor-in-glass for superior high-power artificial plant growth LEDs, J. Mater. Chem. C 6 (2018) 1738–1745.
[13] Z. Wu, A.N. Cormack, Defects in $BaMgAl_{10}O_{17}$: Eu^{2+} blue phosphor, J. Electroceram. 10 (2003) 179–191.
[14] Y. Zheng, W. Zhuang, X. Xing, J. Zhong, R. Liu, Y. Li, Y. Liu, Y. Hu, Synthesis, structure and luminescent properties of a new blue-green-emitting garnet phosphor $Ca_2LuScZrAl_2GeO_{12}$:Ce^{3+}, RSC Adv. 6 (2016) 68852–68859.
[15] J. Zhong, W. Zhuang, X. Xing, R. Liu, Y. Li, Y. Zheng, Y. Hu, H. Xu, Synthesis, structure and luminescence properties of new blue-green-emitting garnet-type $Ca_3Zr_2SiGa_2O_{12}$:Ce^{3+} phosphor for near-UV pumped white-LEDs, RSC Adv. 6 (2016) 2155–2161.
[16] Z. Hao, Y. Wang, L. Zhang, G. Pan, X. Zhang, H. Wu, Y. Luo, J. Zhang, Synthesis and photoluminescence properties of Eu^{2+} activated CaO ceramic powders for near-ultraviolet chip based white light emitting diodes, Opt. Mater. 71 (2017) 1–4.
[17] S. Zhang, Z. Hao, L. Zhang, G. Pan, H. Wu, X. Zhang, Y. Luo, L. Zhang, H. Zhao, J. Zhang, Effcient blue-emitting phosphor $SrLu_2O_4$:Ce^{3+} with high thermal stability for near ultraviolet (~400 nm) LED-chip based white, LEDs Sci. Rep-UK 8 (2018) 1–9.
[18] Z. Hao, X. Zhang, Y. Luo, L. Zhang, H. Zhao, J. Zhang, Enhanced Ce^{3+} photoluminescence by Li^+ co-doping in CaO phosphor and its use in blue-pumped white LEDs, J. Lumin. 140 (2013) 78–81.
[19] Y.T. Tsai, C.Y. Chiang, W. Zhou, J.F. Lee, H.S. Sheu, R.S. Liu, Structural ordering and charge variation induced by cation substitution in (Sr,Ca)$AlSiN_3$:Eu phosphor, J. Am. Chem. Soc. 137 (2015) 8936–8939.
[20] W. Liu, C. Huang, C. Yeh, J. Tsai, Y. Chiu, Y. Yeh, R. Liu, A study on the luminescence and energy transfer of single-phase and color-tunable $KCaY(PO_4)_2$: Eu^{2+}, Mn^{2+} phosphor for application in white-light LEDs, Inorg. Chem. 51 (2012) 9636–9641.
[21] J. Chen, N. Zhang, C. Guo, F. Pan, X. Zhou, H. Suo, X. Zhao, E.M. Goldys, Site-dependent luminescence and thermal stability of Eu^{2+} doped fluorophosphate towards white LEDs for plant growth, ACS Appl. Mater. Interfaces 8 (2016) 20856–20864.
[22] Z. Xia, A. Meijerink, Ce^{3+}-Doped garnet phosphors: composition modification, luminescence properties and applications, Chem. Soc. Rev. 46 (2017) 275–299.
[23] J. Chen, C. Guo, Z. Yang, T. Li, J. Zhao, Li_2SrSiO_4:Ce^{3+}, Pr^{3+} phosphor with blue, red, and near-infrared emissions used for plant growth LED, J. Am. Ceram. Soc. 99 (2016) 218–225.
[24] Y. Wu, D. Wang, T. Chen, C. Lee, K. Chen, H. Kuo, A novel tunable green- to yellow-emitting beta-YFS: Ce^{3+} phosphor for solid-state lighting, ACS Appl. Mater. Interfaces 3 (2011) 3195–3199.
[25] K.B. Kim, Y.I. Kim, H.G. Chun, T.Y. Cho, J.S. Jung, J.G. Kang, Structural and optical properties of $BaMgAl_{10}O_{17}$:Eu^{2+} phosphor, Chem. Mater. 14 (2002) 5045–5052.
[26] J. Deng, H. Zhang, X. Zhang, M.S. Molokeev, J. Qiu, Y. Liu, B. Lei, L. Ma, X. Wang, Enhanced luminescence performance of CaO: Ce^{3+}, Li^+, F^- phosphor and its phosphor-in-glass based high-power warm LED properties, J. Mater. Chem. C 6 (2018) 4077–4086.
[27] H. Li, R. Zhao, Y. Jia, W. Sun, J. Fu, L. Jiang, S. Zhang, P. Pang, C. Li, $Sr_{1.7}Zn_{0.3}CeO_4$: Eu^{3+} novel red-emitting phosphors: synthesis and photoluminescence properties, ACS Appl. Mater. Interfaces 6 (2014) 3163–3169.
[28] J. Zhong, W. Xu, Q. Chen, S. Yuan, Z. Ji, D. Chen, Mn^{4+}, Li^+ co-doped $SrMgAl_{10}O_{17}$ phosphor-in-glass: application in high-power warm w-LEDs, Dalton Trans. 46 (2017) 9959–9968.
[29] G. Li, Y. Tian, Y. Zhao, J. Lin, Recent progress in luminescence tuning of Ce^{3+} and Eu^{2+}-activated phosphors for pc-WLEDs, Chem. Soc. Rev. 44 (2015) 8688–8713.
[30] Z. Mao, J. Chen, J. Li, D. Wang, Dual-responsive Sr_2SiO_4:Eu^{2+}-$Ba_3MgSi_2O_8$:Eu^{2+}, Mn^{2+} composite phosphor to human eyes and plant chlorophylls applications for general lighting and plant lighting, Chem. Eng. J. 284 (2016) 1003–1007.
[31] J. Zheng, Q. Cheng, S. Wu, Z. Guo, Y. Zhuang, Y. Lu, Y. Li, C. Chen, An efficient blue-emitting $Sr_5(PO_4)_3Cl$: Eu^{2+} phosphor for the application in near-UV white light-emitting diodes, J. Mater. Chem. C 3 (2015) 11219–11227.
[32] Z. Zhou, Y. Li, M. Xia, Y. Zhong, N. Zhou, H.T. Hintzen, Improved luminescence and energy transfer properties of $Ca_{14}Al_{10}Zn_6O_{35}$: Ti^{4+}, Mn^{4+} deep-red emitting phosphors with high brightness for light emitting diode (LED) plant growth lighting, J. Mater. Chem. C 47 (2018) 13713–13721.
[33] Y. Kim, P. Arunkumar, B. Kim, S. Unithrattil, E. Kim, S. Moon, J. Hyun, K. Kim, D. Lee, J. Lee, A zero-thermal-quenching phosphor, Nat. Mater. 6 (2017) 543–550.
[34] X. Piao, K. Machida, T. Horikawa, H. Hanzawa, Y. Shimomura, N. Kijima, Preparation of $CaAlSiN_3$:Eu^{2+} phosphors by the self-propagating high-temperature synthesis and their luminescent properties, Chem. Mater. 19 (2007) 4592–4599.
[35] X. Zhang, J. Yu, J. Wang, C. Zhu, J. Zhang, R. Zou, B. Lei, Y. Liu, M. Wu, Facile preparation and ultrastable performance of single component white-light-emitting phosphor-in-glass used for high power warm white LEDs, ACS Appl. Mater. Interfaces 7 (2015) 28122–28127.
[36] J. Deng, W. Li, H. Zhang, Y. Liu, B. Lei, H. Zhang, L. Liu, X. Bai, H. Luo, H. Liu, Eu^{3+}-Doped phosphor-in-glass: a route towards tunable multicolor materials for near-UV high-power warm white LEDs, Adv. Opt. Mater. 5 (2014) 1–9.
[37] X. Zhang, J. Yu, J. Wang, B. Lei, Y. Liu, Y. Cho, R. Xie, H.W. Zhang, Y. Li, Z. Tian, Y. Li, Q. Su, All-inorganic light convertor based on phosphor-in-glass engineering for next-generation modular high-brightness white LEDs/LDs, ACS Photonics 4 (2017) 986–995.
[38] A. Chanwitheesuk, A. Teerawutgulrag, N. Rakariyatham, Screening of antioxidant activity and antioxidant compounds of some edible plants of Thailand, Food Chem. 92 (2015) 491–497.
[39] J. Zhang, L. Dong, S.-H. Yu, A selective sensor for cyanide ion (CN^-) based on the inner filter effect of metal nanoparticles with photoluminescent carbon dots as the fluorophore, Sci. Bull. 60 (2015) 785–791.
[40] S. Zhu, Q. Meng, L. Wang, J. Zhang, Y. Song, H. Jin, K. Zhang, H. Sun, H. Wang, B. Yang, Highly photoluminescent carbon dots for multicolor patterning, sensors, and bioimaging, Angew. Chem. Int. Ed. 52 (2013) 1–6.